



**HAL**  
open science

## Molecular modeling of the mobility of poly(allyl alcohol), PAA, and poly(vinyl alcohol), PVA

A. de la Rosa, Laurent Heux, Jean-Yves Cavaillé, Karim Mazeau

► **To cite this version:**

A. de la Rosa, Laurent Heux, Jean-Yves Cavaillé, Karim Mazeau. Molecular modeling of the mobility of poly(allyl alcohol), PAA, and poly(vinyl alcohol), PVA. *Polymer*, 2002, 43 (21), pp.5665-5677. 10.1016/S0032-3861(02)00471-8 . hal-00475492

**HAL Id: hal-00475492**

**<https://hal.science/hal-00475492>**

Submitted on 1 May 2024

**HAL** is a multi-disciplinary open access archive for the deposit and dissemination of scientific research documents, whether they are published or not. The documents may come from teaching and research institutions in France or abroad, or from public or private research centers.

L'archive ouverte pluridisciplinaire **HAL**, est destinée au dépôt et à la diffusion de documents scientifiques de niveau recherche, publiés ou non, émanant des établissements d'enseignement et de recherche français ou étrangers, des laboratoires publics ou privés.

# Molecular modeling of the mobility of poly(allyl alcohol), PAA, and poly(vinyl alcohol), PVA

A. De La Rosa<sup>a</sup>, L. Heux<sup>a</sup>, J.Y. Cavail  <sup>b</sup>, K. Mazeau<sup>a,\*</sup>

<sup>a</sup>CERMAV-CNRS, Universit   J. Fourier BP 53, F-38041 Grenoble cedex 9, France

<sup>b</sup>GEMPPM INSA-CNRS UMR 5510, F-69621 Villeurbanne cedex, France

Detailed atomistic models of the dense glassy isotactic and syndiotactic poly(allyl alcohol) (PAA) and poly(vinyl alcohol) (PVA) have been simulated and characterized. Models of PVA display very good agreement with experimental characteristic ratio and solubility parameter, whereas no experimental data are available for PAA. Intra- and intermolecular hydrogen bonding interactions for each system were analyzed and compared with available solid-state NMR experiments. The generated microstructures have been used for a quasi-static simulation of localized molecular motions. These motions include the rotation of hydroxyl and hydroxymethyl pendant groups for PVA and PAA, respectively. The average energy barrier of the most probable conformational transition of hydroxymethyl groups in PAA and hydroxyl groups in PVA is estimated to be 45(^13) and 10(^3) kJ mol<sup>-1</sup>, respectively. The mobility of the pendant groups appears to be independent of tacticity. The influence of the side group rotation on the surrounding is very limited. The role of inter- and intramolecular hydrogen bonds is discussed. Mobility of the main-chain backbone is studied in the isotactic PVA model. It is found that the neighboring torsion angles are affected by conformational interconversions of a given backbone angle. This is explained in terms of cooperativity and geometry of the motions. The calculated energy barrier is found at an average value of 52 kJ mol<sup>-1</sup>. The calculated data on the different simulated mobilities are compared with the observed secondary relaxations measured by mechanical spectrometry.

Keywords: Vinyl polymer; Conformational analysis; Molecular mobility

## 1. Introduction

Atomistic modeling appears to be a powerful tool for investigating in detail the effects of molecular structure on local chain dynamics with either Brownian [1], molecular dynamics [2] or variational methods such as the Cooperative Kinematics [3–5]. However, all these methods deal with local dynamics far above  $T_g$ . In the glassy polymers, the chains are frozen and molecular motions involved in the so-called secondary relaxations occur at a much higher time scale. Local packing and conformational effects have a strong impact on these motions. Thus, the modeled systems have to be the most realistic in terms of energy and conformations. So far, several atomistic models of amorphous solid polymers (polycarbonate [6–9], polystyrene [10], polyethylene [11], poly(oxypropylene) [12], etc.) were generated using different methods and with different

purposes, generally with the aim to study macroscopic mechanical properties [7–9,11,12] and transport mechanisms [13–17]. However, the simulation of the molecular mobility was not very often studied. A quasi-static method for localized motions in glassy polycarbonate of 4,4'-isopropylidenediphenol has been presented by Hutnik et al. [6]. Among the literature, studies concerning amorphous polystyrene [18] and cellulose [19] have also been published with this aim. The methodology involves the gradual change of a degree of freedom (a torsion angle) by small increments in order to trace a path in the overall potential energy. Activation energy is then measurable as the height of the barrier necessary to obtain a conformational change. This is an alternative to the molecular dynamics method. Although this method does not correspond to the most realistic description of molecular motion, it could give information on the geometric and energetic features of a given molecular motion. As in the variational method [3–5], it will not give any information on the kinetics of the motion. Keeping these limitations in mind, this quasi-static method appears well

\* Corresponding author. Tel.: +33-4-76-03-76-39; fax: +33-4-76-54-72-03.

*E-mail address:* karim.mazeau@cermav.cnrs.fr (K. Mazeau).

adapted to give new insights on the molecular motions occurring in the glassy state.

In this context, we are interested in the description of the molecular motions in polymers bearing polar side groups. This large family includes the widespread polysaccharides, like cellulose or amylose for example. For cellulose, low temperature relaxations were measured by dynamic mechanical analysis (DMA) [19] and dielectric spectrometry [20]. In preceding works, we have shown that polysaccharides and vinyl polymers bearing polar side groups share some common dynamical features [21,22]. These two polymers, poly(vinyl alcohol) (PVA,  $-(\text{CH}_2\text{CH}(\text{OH}))_n-$ ) and poly(allyl alcohol) (PAA,  $-(\text{CH}_2\text{CH}(\text{CH}_2\text{OH}))_n-$ ), were characterized by mechanical [21] and dielectric [22] spectrometry. Localized non-cooperative motions of the side groups were related to the low temperature relaxation process ( $\gamma$ ) observed in polymers presenting  $\text{CH}_2\text{OH}$  side groups (cellulose and PAA). The differences between hydroxyl and hydroxymethyl moieties have been attributed to differences in the inertial moment of the two groups, but it still remains a hypothesis which can be tested by computational techniques. On the other hand, a common secondary relaxation ( $\beta$ ) preceding the glass transition was measured for all polymers (vinyl polymers and polysaccharides). Generally, the  $\beta$ -relaxation is explained on the basis of slight cooperative motions of the main-chain by opposition with the  $\alpha$ -relaxation which is highly cooperative. The potential existence of such slightly cooperative motions can also be tested by the quasi-static method.

In this work, we first report the generation of static microstructures of the isotactic and syndiotactic PVA and PAA in their dense amorphous state. Then, we have studied localized motions. The general strategy relies on the aforementioned quasi-static model for localized motions. These motions include the rotation of hydroxyl and hydroxymethyl groups of PVA and PAA, respectively, and the main-chain motion. The aim of this work is therefore to discuss the statistical results obtained for the energy profiles on the basis of experimental measurements of mechanical relaxations. The detailed analysis of the geometry and cooperativity of the motions should give better insights in the molecular origin of the relaxation process for polymers bearing polar side groups.

## 2. Simulation details

### 2.1. Force field

Energy calculations were carried out by using the second-generation force field PCFF [23–26] specially suited for polymers and other organic materials. The PCFF force field is an augmented version of the ab initio consistent force field (CFF91) for which new functional groups were added. It has been parametrized and validated

using condensed phase properties in addition to various ab initio and empirical data for molecules in isolation.

The bound terms of the potential energy function include a quadratic polynomial for both bonds stretching and angle bending, a three-term Fourier expansion for torsions and a Wilson out of plane coordinate term. Six crossterms up to the 3rd order are present to account for coupling between the intramolecular coordinates. The final two non-bonded terms use a Coulombic form for the electrostatic energy and an inverse 6–9th power Lennard-Jones function is used for the van der Waals term. For the Coulombic term, the dielectric constant value was set to 1. All atoms are treated explicitly. The van der Waals and electrostatic non-bonded interactions were calculated by the Ewald’s method with an accuracy value of  $2.5 \times 10^{-4}$  kcal mol $^{-1}$ .

The suitability of those two force field to model polyols have been assessed by other authors. The systems studied were poly(vinyl phenol) [27] and starch with different moisture content [28,29]. In good concordance with experimental studies, it was shown that the interactions, dominated by polar groups are correctly described. Additionally, a new method to estimate equilibrium water content of wet PVA was developed by using the PCFF force field [30].

### 2.2. Structure generation

Exploration of the conformational characteristics of representative skeletal fragments of the polymers is a prerequisite to adequately model larger fragments. The fragment molecules are the 2*R*,4*S* pentanediol (syndiotactic PVA, s-PVA), the 2*R*,4*R* pentanediol (syndiotactic PAA, s-PAA), the 2*R*,4*S* dimethyl 1,5-pentanediol (isotactic PVA, i-PVA) and 2*R*,4*R* dimethyl 1,5 pentanediol (syndiotactic PAA, s-PAA). Although the conformational analysis of PVA has been reported by Wolf and Suter [31], it has to be re-evaluated to remain consistent in the analysis throughout the same force field.

Ramachandran-type conformational energy maps were computed for all the above mentioned structures. The conformational energy was calculated as a function of skeletal torsion angles for every 5° in the interval from 0 to 360°. For each conformational state of the backbone, a geometry optimization is performed by allowing all the Cartesian coordinates to vary except those defining the ( $\phi_1$ ,  $\phi_2$ ) torsion angles. The minimization was performed with standard conjugate gradient method with convergence criteria of 0.02 kcal mol $^{-1}$  Å $^{-1}$  for rms of the force. Three initial orientations (60, 180 and 300°) are defined for each of the torsions defined from the two pendant groups ( $\omega_1$ ,  $\omega_2$ ) in the fragments (see Fig. 1(a) and (b) for the definitions of the torsion angles). So, nine initial conformations are build for each dyad with a different position to pair of side groups and nine different Ramachandran-type conformational energy maps were calculated exploring all the relevant possibilities of the staggered orientations of the pendant groups. Among

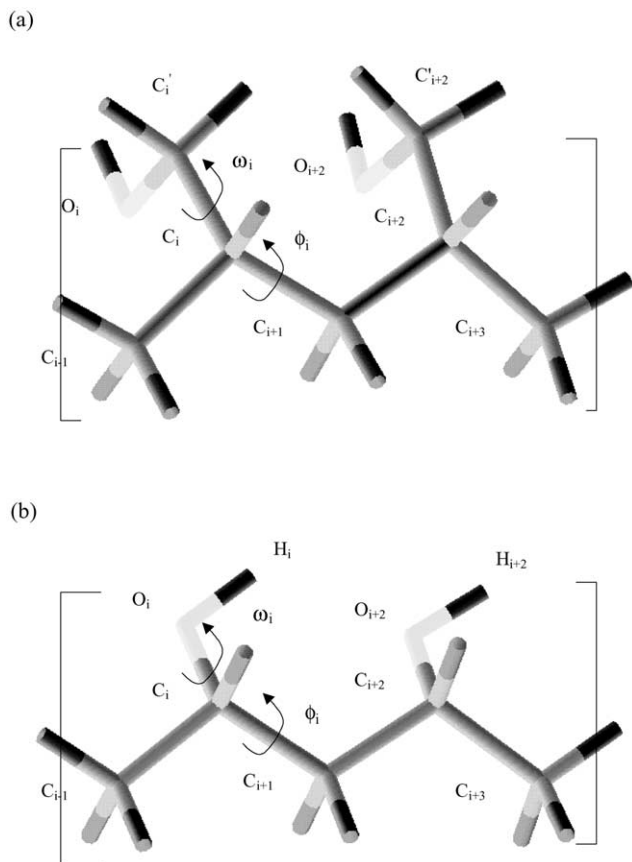


Fig. 1. Schematic drawing of the segments of PAA (a) and PVA (b) chains along with the definition of the relevant side group ( $\omega_i$ ) and skeletal ( $\phi_i$ ) torsion angles.

them, the lowest energy was then chosen as the final value used in the generation of the polymer chains.

Model microstructures of both PVA and PAA were generated. The influence of the tacticity was explored by generating, for both polymers, isotactic and syndiotactic structures: isotactic PVA (i-PVA), isotactic PAA (i-PAA), syndiotactic PVA (s-PVA) and syndiotactic PAA (s-PAA). So, four different ensembles containing 25 conformations each were constructed. In each case, the polymer is represented as an ensemble of cubic microscopic structures for which periodic continuation conditions are employed. The first repeat unit was filled into the box by choosing place and orientation at random. Then, a random conformation of a polymer having a degree of polymerization of 100 was built one residue at a time within the cell.

The angles for the skeletal torsion were assigned by the normalized Boltzmann abundances of each conformational state at 300 K, calculated from the potential energy surfaces of the model fragments. For those generated structures, the torsion angles are allowed to be dispersed by  $20^\circ$  around their optimal values. A conformation is accepted if the generated residue is free of strong steric clashes with all the previously generated ones. Note that the temperature used is below the experimental  $T_g$  of the polymers (353 and 348 K [21,22], respectively). Those models are static by nature;

temperature is evoked only indirectly through both the Boltzmann probability of each conformational state used by the Metropolis Monte-Carlo procedure and through the density at which structures are generated.

The measured density at room temperature of atactic PVA is  $1.293 \text{ g cm}^{-3}$  [32] and for PAA  $1.28 \text{ g cm}^{-3}$  estimated by volume-weight relationships in dried PAA fibers. Dimensions of the cells depended on the experimental density. The cube edges were then 17.8 and  $19.6 \text{ \AA}$  for PVA and PAA, respectively.

As segments were added to the growing chain, the non-bond distances of the conformation generated were checked. To facilitate the generation of the polymer within the box, a scale factor of 0.3 was applied to all the van der Waals interactions in this first stage of the generation. The minimum non-bond distance allowed is equal to the sum of the two atom's van der Waals radii multiplied by this specified scale factor.

### 2.3. Structure equilibration

Each generated structure is then relaxed to a local state of minimal potential energy. This process of minimization was performed by two different minimization methods: first, the steepest descents and then the conjugate gradient.

A straightforward energy minimization scheme is likely to trap the simulated system in a metastable local high-energy minima. Molecular dynamics simulation was used to prevent the system from such entrapments by providing thermal energies to cross energy barriers between local minima. This was performed on two randomly chosen structures of each polymer. A relaxation cycle was used, consisting of a 50 ps NVT dynamics run in which the temperature is gradually decreased from 600 to 300 K, followed by an energy minimization run. Then another 50 ps dynamics in the NPT ensemble in which the simulation box was allowed to vary in size and shape in order to find the equilibrium density for each structure. This was again followed by an energy minimization.

The convergence criteria used for energy minimizations was a root-mean-square (rms) force less than  $0.1 \text{ kcal mol}^{-1} \cdot \text{\AA}^{-1}$  for the polymer and  $0.1 \text{ kcal mol}^{-1} \cdot \text{\AA}^{-3}$  for the stresses on the periodic boxes. Both convergence criteria were simultaneously satisfied for the system to be relaxed completely.

The standard Verlet [33] algorithm was used to integrate Newton's law of motion with a time step of 0.001 ps. For the canonical NPT dynamics [34], the relaxation time constant and the masslike parameter which determines the rate of change of volume/shape matrix were set to 0.1 ps and 1.00, respectively. Each molecular dynamics run was started by assigning initial velocity for the atoms according to Boltzmann distribution at 600 K. The velocities of the atoms were quickly scaled down so that the final temperature of atoms was 300 K. The total external pressure was maintained at 1 atm, and Nosé's algorithm [35] was

used to keep the cell temperature constant at 300 K in the molecular dynamics simulation.

Those short-run molecular dynamics were performed in order to relax the bulk structure efficiently by introducing thermal motions to cross any energy barriers between local minima.

Energy evaluation, molecular dynamics and minimization procedures were performed using the commercial molecular simulation software Cerius<sup>2</sup> [36]. All calculations were carried out on Silicon Graphics workstations.

Table 1 lists the average values of six internal stress tensors in the simulation boxes during the equilibration process. The internal stress components,  $ij$ , are defined as the first derivative of the potential energy per unit volume with respect to strains. At equilibrium, these values must be close to zero, and any high positive or negative values indicate that the system is under tension or compression. Table 1 shows the internal stress in units of MPa, and the low values obtained on both the (NVT) and the (NPT) relaxation cycles suggest that the mechanical equilibrium is reached as early as the end of the first NVT cycle. The polymer structures are correctly relaxed.

The simulation cell parameters were allowed to vary during the final NPT step of the relaxation, and the average cell dimensions increases leading to a lower density than expected. The optimized densities of the PAA and PVA polymers were found to be 1.14 (s-PAA), 1.17 (i-PAA), 1.14 (s-PVA) and 1.21 (i-PVA)  $\text{g cm}^{-3}$ . These densities are somewhat lower than the experimental values of 1.28 and 1.29  $\text{g cm}^{-3}$  determined for PAA and PVA, respectively. An additional pressure should have been used to reach the correct density as in the case of amylose [28]. To avoid this density discrepancy and the use of high pressure, the remaining study was performed on structures that have been equilibrated by using the NVT dynamics as suggested by numerous authors [37–40].

These amorphous structures were used to study two types of molecular motions. First, the independent simple rotations of hydroxyl and hydroxymethyl side groups were

Table 1  
Internal stress tensors (MPa) of the simulated boxes during the equilibration protocol

	XX	YY	ZZ	YZ	XZ	XY
s-PAA	2.42	2.40	2.44	0.02	-0.02	0.02
NVT	-0.17	0.28	-0.10	0.01	-0.15	-0.05
NPT	0.05	-0.30	0.24	-0.08	0.04	0.09
i-PAA	2.66	2.66	2.68	0.04	-0.04	-0.03
NVT	1.49	1.05	1.24	-0.09	0.01	-0.04
NPT	0.00	-0.01	0.02	-0.09	-0.07	-0.07
s-PVA	1.52	1.54	1.56	0.00	-0.02	0.00
NVT	0.14	0.48	0.26	0.06	-0.03	0.04
NPT	-0.13	0.33	-0.20	-0.07	0.00	0.31
i-PVA	1.62	1.71	1.72	0.01	-0.02	0.02
NVT	0.23	0.28	0.34	0.03	0.04	0.05
NPT	0.12	-0.05	-0.06	-0.14	-0.09	-0.06

simulated for the two different tacticities in both systems. Then the rotation of skeletal torsions in isotactic PVA (i-PVA) was also studied.

#### 2.4. Modeling the side group motion

Fig. 1(a) and (b) shows a sequence of the two repeat units of i-PAA and i-PVA, respectively. The torsion angle of interest is  $\omega_i$ , defined by  $C_{i-1}-C_i-C'_i-O_i$  and  $C_{i-1}-C_i-O_i-H_i$  atoms for PAA and PVA, respectively.

A degree of freedom ( $\omega_i$ ), is selected and changed by a small amount and then held to this new value. We found that the optimal torsion step is  $10^\circ$ , lower values did not change the results while the profiles are badly defined for larger values. All other degrees of freedom in the system are adjusted by minimization of the potential energy of the microstructure. This minimization process is subjected, however, to the requirement that the chosen degree of freedom remains unchanged. A conformational path is then traced. It shows the variations of the overall potential energy as a function of the chosen degree of freedom.

Fifty hydroxyl side group torsions in each i-PVA and s-PVA structure and fifty hydroxymethyl side group torsions in each i-PAA and s-PAA structure were studied.

#### 2.5. Modeling the main-chain motion

Variation of the skeletal torsion angles was modeled by a quasi-static method in which a single torsion ( $\phi_i$ , defined by four consecutive  $C_{i-1}-C_i-C_{i+1}-C_{i+2}$  atoms in PVA) (Fig. 1(b)) is forced to adopt a new value during the minimization process. The strategy that was used to study the side group motions is not applicable in the present case. The chain-ends molecular movements that arise from a  $10^\circ$  variation of an inner skeletal torsion angle are very large, leading to dramatic increases in the potential energy of the system because of strong atom overlapping. To prevent this, another strategy was adopted. A chosen torsion angle is forced to reach a new value during the minimization by using harmonic restraints as an additional torsional term of the potential energy function. Here again, the  $10^\circ$  step size was found to be the optimal value. The force constant is of  $1000 \text{ kcal (mol rad}^2\text{)}^{-1}$ . This additional force leads to an increase of the total potential energy of the system to about  $20 \text{ kcal mol}^{-1}$  ( $\approx 84 \text{ kJ mol}^{-1}$ ) for a torsion of  $10^\circ$  ( $\approx 0.175 \text{ rad}$ ) which after minimization falls down to around  $0.1 \text{ kcal mol}^{-1}$ . Therefore, the change of  $\phi_i$  does occur during the minimization process. Fifty skeletal torsion angles in i-PVA were studied by this method.

### 3. Results and discussion

#### 3.1. Bulk static properties

According to Flory's hypothesis [41–43], the chain in

Table 2

Probabilities (%) of the  $\phi$  skeletal torsion angle from model fragment (frag) and corresponding distribution (%) for equilibrated isotactic and syndiotactic structures of PVA and PAA

	$g^+$	$t$	$g^-$		$g^+$	$t$	$g^-$
PVA frag	9.1	72.2	13.7	PAA frag	49.0	49.7	1.3
PVA iso	19.4	64.6	16.0	PAA iso	42.3	45.4	12.3
PVA frag	25.0	73.7	1.3	PAA frag	1.6	67.7	30.7
PVA syn	25.7	57.6	16.7	PAA syn	28.0	51.0	21.0

the melt or in the glassy state is supposed to share the same conformational statistics as in the  $\theta$  conditions. The torsion angles values are a local indicator of the conformational characteristics of the chain. The distribution of the conformation angles of the equilibrated structures are described by a Gaussian function centered at the canonical staggered values with a full width at half-height between 40 and 50°.

Table 2 compares the conformational states distribution of the skeletal bond between the model fragment and the dense microstructures. Slight departures from the expected populations are observed. This seems to be a consequence of steric intermolecular interactions in the bulk state that were absent in the calculations of the model fragments. Note that this effect was also observed for polystyrene [10] and poly(vinyl chloride) [44] simulations and recently analyzed by Robyr [40]. In the case of PVA and PAA, although some minor states are more populated than anticipated, the overall probabilities of each state is globally respected. The same trend was observed on polypropylene [45], for which the side group (CH<sub>3</sub>) has a size between those of hydroxyl and hydroxymethyl. The satisfactory agreement concerning the population of the different conformational states between the model fragments and the generated polymer suggests that the generated conformations are close to the expected unperturbed state.

The average dimension of the chains, pictured by the characteristic ratio, is a measure of their conformation. The reported experimental data of atactic PVA diverge substantially. Evaluating the combined literature on experimental data, Suter and Wolf [31] suggested a reasonable experimental value of the characteristic ratio of PVA in water of  $C_\infty = 8.5$ . The calculated values, using matrix generation techniques [31] for isotactic, syndiotactic and atactic (having a weight fraction of meso diad of 0.5) PVA isolated chains are 7.8, 12.2 and 9.5, respectively.

The average values of  $C_{200}$  of the minimized structures are 8.9 and 11.3 for i-PVA and s-PVA, respectively. Our generated models show a good agreement with those previous studies, especially the differences between isotactic and syndiotactic dimensions. This supports the general relevance of the generation procedure.

On the other hand, there is no experimental data for PAA. The calculated characteristic ratio is found at  $C_{200} = 8.1$  and 11.0, for the isotactic and syndiotactic form, respect-

ively. The influence of the tacticity is the same for PVA and PAA, and their overall shape and dimensions are not very different, essentially governed by the flexibility of the vinyl backbone.

The cohesive energy,  $E_{\text{coh}}$  is defined as the intermolecular part of the internal energy  $U$  per mole of substance. The cohesive energy density corresponds to the cohesive energy per unit of volume. Hildebrand’s solubility parameter,  $\delta$ , is the square root of the cohesive energy density. As those parameters strongly depend on the force field used and on the precise generated microstructure, it should represent another good test of the physical relevance of our models.

The reported experimental value for the solubility parameter of atactic PVA is  $12.6 \text{ (cal cm}^{-3}\text{)}^{1/2}$  [46]. In very good agreement with this experimental data, our simulations gives values of  $12.3 \pm 0.4$  and  $13.6 \pm 0.6 \text{ (cal cm}^{-3}\text{)}^{1/2}$  for i-PVA and s-PVA, respectively. Such an agreement suggests that the simulation methodology together with the choice of the force field correctly reproduce the experimental data from an energetic point of view. The same calculation leads to values of  $12.4 \pm 0.6$  and  $12.3 \pm 0.4 \text{ (cal cm}^{-3}\text{)}^{1/2}$  for i-PAA and s-PAA for which no experimental data are available.

### 3.2. Hydrogen bonding interactions

An hydroxyl–oxygen pair is generally considered to be hydrogen-bonded if geometrical criteria on the OH $\cdots$ O distance and angle are satisfied. Considering the calculated radial distribution function (not shown), we choose an OH $\cdots$ O distance smaller than 2.5 Å and an angle between O–H $\cdots$ O atoms higher than 90° for further analysis of the hydrogen bonds. Table 3 summarizes some hydrogen bonding averaged features. These results are also compared with those of the literature [28,47]. For each system, each hydroxyl participates on average at least at 0.75 and on maximum at 0.97 hydrogen bonds.

Three types of hydrogen bonds have to be distinguished: (i) ‘neighboring intramolecular’ hydrogen bonds which involve two consecutive polar groups in the chain, (ii) ‘remote intramolecular’ hydrogen bonds between distant monomers of the same chain in spatial proximity, and (iii) ‘intermolecular’ hydrogen bonds, which involve repeat units of different chains.

All the systems but i-PVA shows few intramolecular hydrogen bonds and many intermolecular ones. For i-PVA, the intramolecular hydrogen bonds represent about 60% of the total. Most of them are neighboring hydrogen bonds. A succession of  $t$  conformation of the backbone torsion angles particularly favors the occurrence of hydrogen bonds chain. For s-PVA, the average number of intramolecular hydrogen bond is lower, while maintaining the same ratio between neighboring and remote hydrogen bonds. This polymer also exhibits a large number of intermolecular hydrogen bonds.

Table 3

Total, intra- and intermolecular hydrogen bonds amounts for PVA and PAA systems. Comparison between calculated (calcd) and experimental (exp.) results

System	Type	Total <sup>a</sup>	Intramolecular <sup>a</sup>			Intermolecular <sup>a</sup>	Reference
			Total	Neighboring	Remote		
i-PVA	Calcd	0.97	0.56 (58%)	0.47	0.08	0.41 (42%)	This work
s-PVA	Calcd	0.88	0.27 (31%)	0.21	0.05	0.59 (69%)	This work
i-PVA	Exp.	–	0.56			–	[47]
s-PVA	Exp.	–	0.24			–	[47]
i-PAA	Calcd	0.75	0.16 (21%)	0.04	0.12	0.57 (79%)	This work
s-PAA	Calcd	0.76	0.23 (30%)	0.12	0.11	0.53 (70%)	This work
Amylose	Calcd	2.47 <sup>a</sup>	1.18 (48%)			1.29 (52%)	[28]
		1.96 <sup>b</sup>	0.53 <sup>b</sup> (27%)			1.43 <sup>b</sup> (73%)	

<sup>a</sup> Number of hydrogen bonds per hydroxyl group.<sup>b</sup> Number of hydrogen bonds per hydroxymethyl group.

The presence of a chain of hydrogen bonds occurs consequently to a lesser extent.

These results are also compared in Table 3 to experimental values obtained by CP/MAS <sup>13</sup>C NMR by Horii et al. [47] on PVA with different tacticities. The line arising from the CH resonance splits into three peaks attributed to the formation of two, one or no hydrogen bonds. According to these authors, this splitting concerns only the intramolecular hydrogen bonds. From the integrals of these peaks, it is possible to obtain an average number of hydrogen bonds by hydroxyl group. The NMR results show a great difference between s-PVA and i-PVA, with twice hydrogen bonds in the latter. The calculated data are in very good agreement.

For PAA, intermolecular hydrogen bonds are of extreme importance (79 and 70% for i-PAA and s-PAA, respectively). The absence of chains of hydrogen bonds like in i-PVA is related to the tortuosity in the chain folding.

### 3.3. Rotation of side groups

#### 3.3.1. Energy profiles

Typical energy profiles for the conformational transitions of selected OH and CH<sub>2</sub>OH side groups for s-PAA and s-PVA are shown in Figs. 2 and 3, respectively. The isotactic and syndiotactic forms share the same behavior. Each side

group rotation shows a specific energy profile, which depends on the local environment of the group. The presented plots are chosen as representative examples. One, two or three energy minima can be seen on the plots. The energy minima can be similar or very different in energy. No sharp discontinuities were seen on the energy profiles. Moreover, two successive conformational path performed on the same side group have the same trace after two or three successive rotations of 360°. Finally, the shape of the energy profiles obtained by positive increments is the same as those obtained with negative increments. This should ensure the reversibility of the quasi-static process.

Those energy profiles are a good representation of the well-known ‘two-sites jump’ model, in which a motion is considered between two equally populated sites separated by an energy barrier. A transition is then considered possible if the path shows, besides the starting conformation, another stable position. Two different minima were considered equivalent when the Boltzmann probability ( $P_j$ ), at 300 K, of transition from one to the other is equal or higher to 10%, which corresponds to a difference in energy of ca. 5.5 kJ mol<sup>-1</sup>. In those cases, the increase in the potential energy from the unconstrained ‘ground state’ to the upper point represents the energy barrier ( $E_a$ ) for which the system has to be activated. Average characteristics of the studied motions are reported in Table 4.

Table 4

Statistical characteristics of the modeled side group (hydroxyls and hydroxymethyls) mobility in PAA and PVA. Comparison with simulated amorphous cellulose

System	Cases with $m > 1$ (%) <sup>a</sup>	Cases with $P_j \geq 10\%$ <sup>b</sup> (%)	$E_a$ (kJ mol <sup>-1</sup> )	Reference
i-PAA	98	20	41(±14)	This work
s-PAA	96	26	44(±19)	This work
Cellulose	–	18	40(±10)	[1]
i-PVA	32	8	10(±3)	This work
s-PVA	44	8	13(±2)	This work

<sup>a</sup> Number of energy profiles with more than one minimum.<sup>b</sup> Proportion of equivalent minimum.

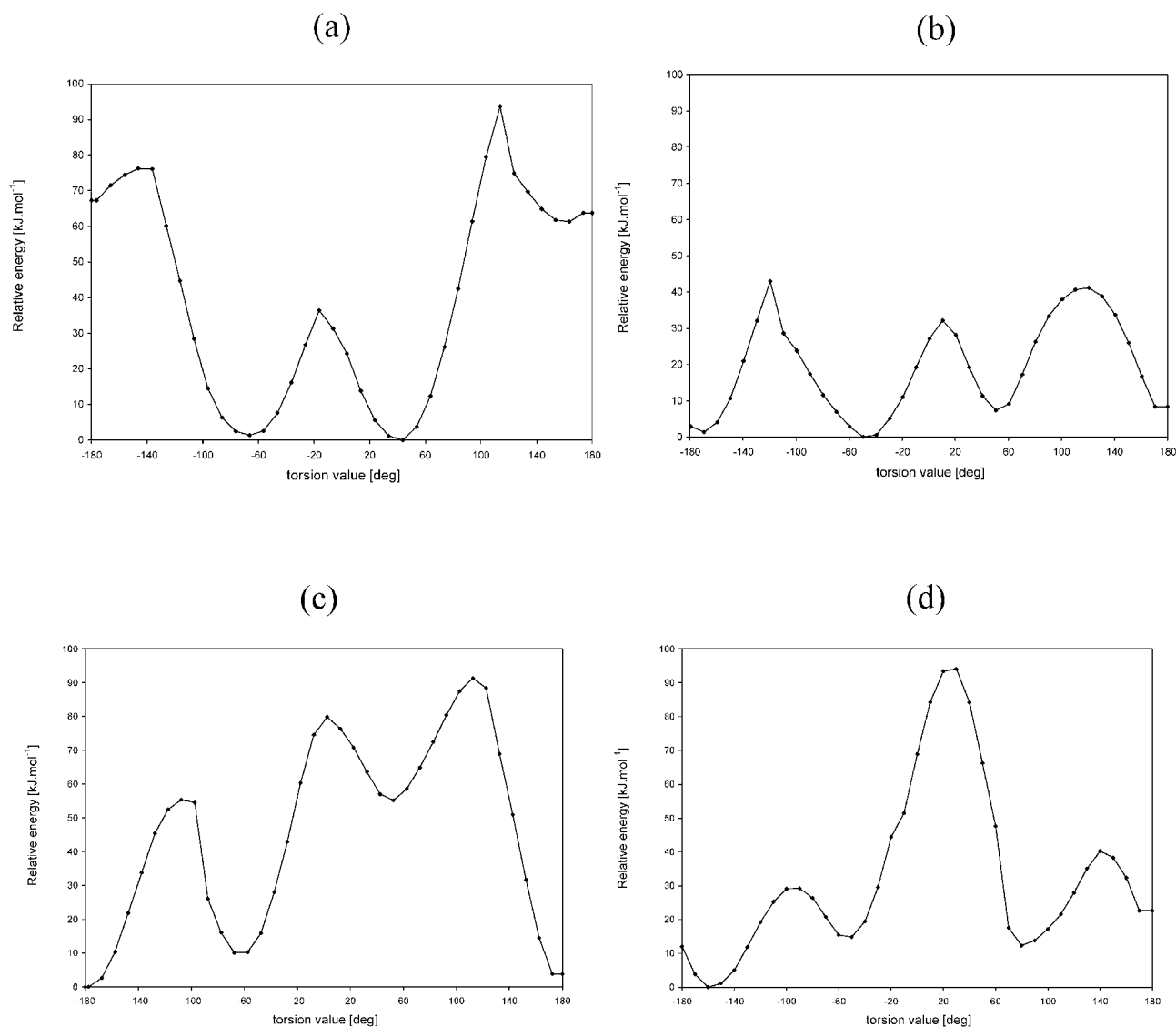


Fig. 2. Representative energy profiles for side chain torsion angles ( $\omega_i$ ) variation in s-PAA:  $\omega_{68}$  (a),  $\omega_{108}$  (b),  $\omega_{144}$  (c) and  $\omega_{148}$  (d).

For PAA, most of the side groups can adopt two or three stable orientations (Fig. 2). The calculated data shows that 98 and 96% of the fifty side groups have at least two energy minima in their energy profiles for the isotactic and syndiotactic forms, respectively. Among the total studied cases, only 20 and 26% of them have equivalent energy minima with an average energy barrier of  $43(\pm 12)$  and  $47(\pm 15)$   $\text{kJ mol}^{-1}$ , respectively. For example, Fig. 2(a) shows a probable transition between the  $g^-$  and  $g^+$  states and Fig. 2(b) between the  $g^-$  and  $t$  states.

The behavior of the PVA hydroxyls is quite different from that of hydroxymethyls in PAA. For i-PVA and s-PVA, about 60% of the hydroxyl side groups of PVA present a unique stable conformation (Fig. 3(a)–(c)); the two other staggered orientations do not correspond to energy minima. Thus, 32 and 44% of the groups have distinct minima and only 8% are equivalent with an average energy barrier of  $10(\pm 3)$  and  $13(\pm 2)$   $\text{kJ mol}^{-1}$ . Therefore,

only 8% of the overall sites in PVA are able to undergo a conformational motion that would lead to a relaxation process.

### 3.3.2. Cooperativity of the motion

The geometrical consequences of a localized side group conformational transition within the chain can be analyzed by the maximal and the average variation for all side groups ( $\Delta\omega_{\text{max}}$  and  $\Delta\omega_{\text{av}}$ ) and skeletal ( $\Delta\phi_{\text{max}}$  and  $\Delta\phi_{\text{av}}$ ) torsion angles along the chain. They are reported in Table 5. The studied torsion angle varies about  $120^\circ$  to go from a staggered conformation to another ‘equivalent’ conformation. For both side groups and skeletal torsion angles,  $\Delta\omega_{\text{av}}$ , and  $\Delta\phi_{\text{av}}$  are negligible during the conformational change of the studied side group, and  $\Delta\omega_{\text{max}}$  and  $\Delta\phi_{\text{max}}$  do not exceed  $10^\circ$ . Independent of the polymers, the variations of the studied torsion angle have little consequences on the remaining part of the chain. The side group motions can

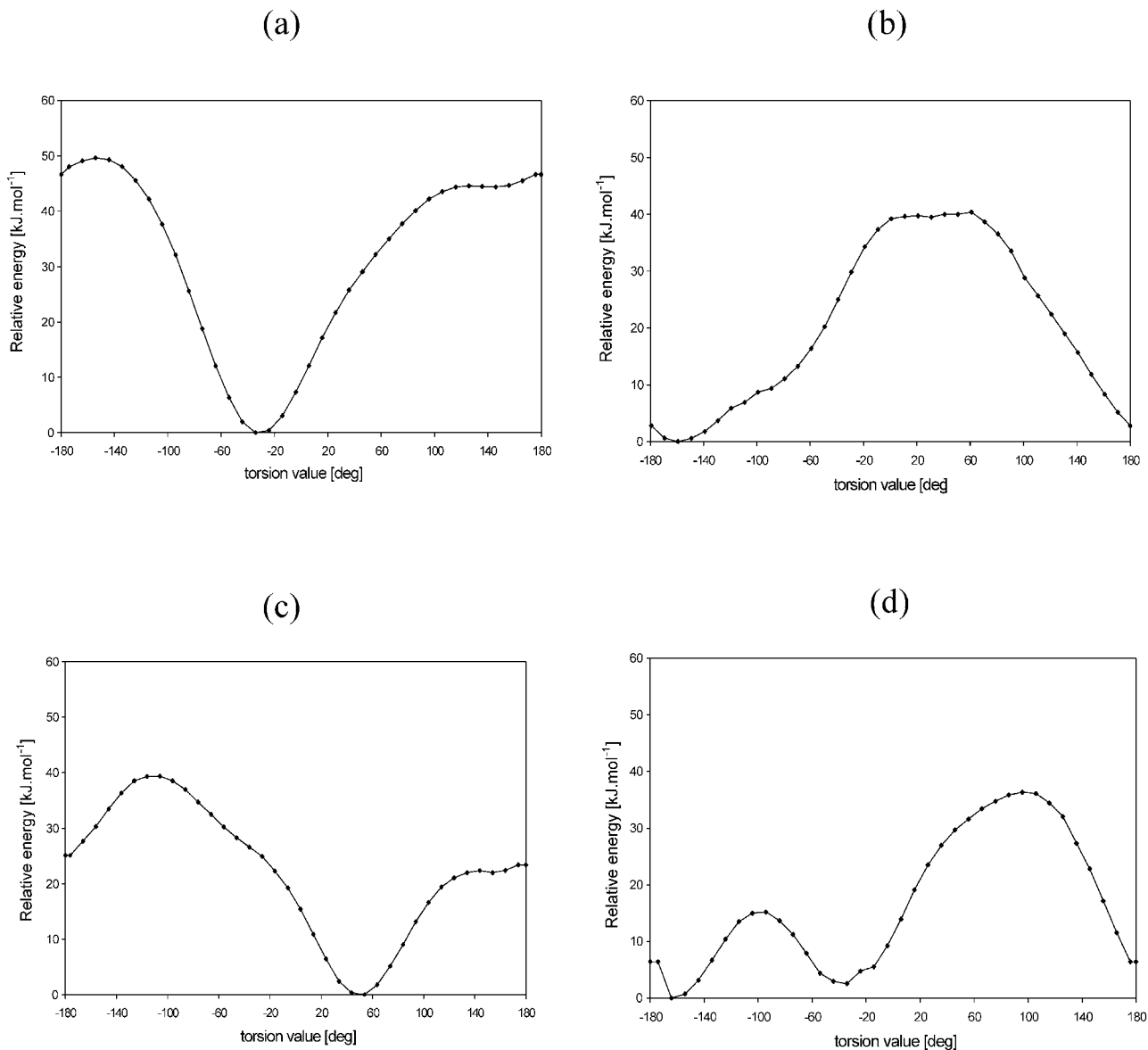


Fig. 3. Representative energy profiles for side chain torsion angles ( $\omega_i$ ) variation in s-PVA:  $\omega_{110}$  (a),  $\omega_{120}$  (b),  $\omega_{150}$  (c) and  $\omega_{52}$  (d).

Table 5

Typical variation of the remaining torsion angles along the chain (see text) when a side ( $\omega$ ) or skeletal ( $\phi$ ) specific bond undergo a conformational change ( $120 \pm 20^\circ$ ) between two equivalent positions

Restrained torsion	$(\Delta\phi)_{av}$ ( $^\circ$ )	$(\Delta\phi)_{max}$ ( $^\circ$ )	$(\Delta\omega)_{av}$ ( $^\circ$ )	$(\Delta\omega)_{max}$ ( $^\circ$ )	$N(\phi)^a$	$N(\omega)^b$
$\omega^c$	0.7	7.3	0.8	8.2	0	0
$\omega^d$	0.2	2.0	0.5	5.4	0	0
$\phi^e$	3.8	22.0	6.4	63.4	2	3–5
$\phi^f$	3.0	20.0	6.3	59.0	4	4–6

<sup>a</sup> Number of neighboring skeletal torsion angles presenting a simultaneous conformational change.

<sup>b</sup> Number of neighboring side chain torsion angles presenting a simultaneous conformational change.

<sup>c</sup> Typical hydroxymethyl side chain torsion.

<sup>d</sup> Typical hydroxyl side chain torsion.

<sup>e</sup> Typical skeletal torsion in PVA for a  $t$  to  $g^-$  conformational change.

<sup>f</sup> Typical skeletal torsion in PVA for a  $g^+$  to  $t$  conformational change.

occur without simultaneous conformational variations of the polymer. The motions of both hydroxyls and hydroxymethyls remain localized, and this suggests an absence of cooperativity. Indeed, the reversibility of the quasi-static process can be related to the non-cooperative character of the relaxation.

### 3.3.3. Comparison with experimental results

On one hand, a weak non-cooperative mechanical relaxation ( $\gamma$ ) is observed by DMA for dried PAA at low temperature with an apparent activation energy of  $45(\pm 7) \text{ kJ mol}^{-1}$  [21]. This is in very good agreement with the calculated data and with the previous calculation on hydroxymethyl motions in cellulose (Table 4). However, the calculated data reveals that few groups (around 20%) are able to undergo a conformational change. This could

explain why the amplitude of the  $\gamma$ -relaxation measured by DMA is so weak. Moreover, the motion can occur without rearrangement of the backbone. This well corresponds to the idea of a localized and non-cooperative relaxation. Finally, the isotactic and syndiotactic forms of PAA share the same characteristics. If, as a first approximation, amorphous (i.e. mainly atactic) PAA can be considered as a statistic copolymer of isotactic and syndiotactic sequences, then the results observed above can be extended for atactic PAA, which seems to be confirmed by the good agreement between experimental data and simulation.

On the other hand, no detectable secondary  $\gamma$ -relaxation can be measured for dried PVA by DMA [21]. The simulated data indicate that almost all the hydroxyls of PVA are unable to undergo a conformational change, as they only exhibit one minimum in their energy profile. Moreover, the few side groups that could lead to a relaxation process have to cross barriers of only  $10 \text{ kJ mol}^{-1}$ . This value is too low to give rise to an observable relaxation process in the time–temperature scale probed by DMA with our experimental conditions. Indeed, assuming an Arrhenius behavior, a non-cooperative relaxation process with an activation energy of  $10 \text{ kJ mol}^{-1}$  will occur at around 40 K for a frequency of 1 Hz.

### 3.3.4. Influence of hydrogen bonding

The analysis of the motional behavior of the lateral groups in PVA and PAA shows important differences with regard to this aspect. The majority of the hydroxyl groups (56–68%) of s-PVA and i-PVA, respectively, exhibits a unique low-energy position. As aforementioned, PVA is mainly stabilized by intramolecular hydrogen bonds, most of them occurring between nearest neighbors. These neighboring intramolecular hydrogen bonds make improbable the existence of a second minimum, which is suppose to break this rigid hydrogen bonds network. The remaining hydroxyl groups (32–44%) presents two or three low-energy positions and only 8% have two equivalent energy minima separated by a low-energy barrier. This situation corresponds rather to hydroxyls having either intermolecular or remote intramolecular hydrogen bonds.

On the other hand, a very high percentage (98%) of the hydroxymethyl groups of PAA has two or three low-energy positions (Table 4). Furthermore, the amorphous structure of PAA is stabilized by intermolecular or remote intramolecular hydrogen bonds. Neighboring intramolecular hydrogen bonds like in PVA are of lower occurrence and makes improbable the existence of a hydrogen bonds network. Thus, various situations of relaxation are encountered. Between two equivalent minima, the  $\text{CH}_2\text{OH}$  group can either be stabilized by one or several intermolecular or remote intramolecular hydrogen bonds.

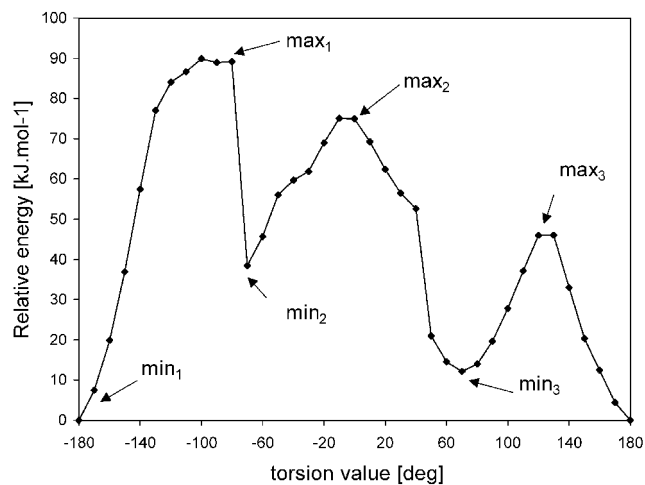


Fig. 4. Representative energy profiles for a skeletal torsion angle ( $\phi_{90}$ ) variation in i-PVA. Barriers transitions (barrier  $i$  for  $i = 1, 2$  and  $3$ ) are defined between positions  $\text{min}_i$  and  $\text{max}_i$ .

## 3.4. Motion of the main-chain

### 3.4.1. Energy profiles

For the i-PVA amorphous solid, a total of fifty main-chain bonds have been selected for the conformational space searching. To avoid chain-ends artifacts, the bonds have been chosen in the center of the chain. A typical energy profile as a function of the skeletal torsion angle values is shown in Fig. 4. The angular increments are positive. The shapes of the curves are radically different from those obtained in the case of the side group motions. Sharp discontinuities of the energy profiles are observed in most cases for those skeletal motions. The brutal change of the total potential energy occurs frequently around the maxima. However, in 84% of the cases the energy profile shows three low-energy positions corresponding to the three staggered conformational states:  $t$  ( $180^\circ$ ),  $g^+$  ( $60^\circ$ ) and  $g^-$  ( $-60^\circ$ ). In 68% of the cases, the  $t$  orientation is the lowest energy conformation (Table 6). This corresponds to the preferred  $t$  state in the initial minimized structure. The total energy first increases from the minimum (called  $\text{min}_1$ ) to a maximal value ( $\text{max}_1$ ). After the first maximal energy value, a second ( $\text{min}_2$ ) and third ( $\text{min}_3$ ) minimal and maximal values ( $\text{max}_2$  and  $\text{max}_3$ ) are observed (in the positive direction, i.e. from left to right). Another fundamental difference with the side group rotation is the irreversibility of the quasi-static process. Two successive rotations of the main-chain skeletal torsion do not give the same trace. Moreover, the energy profiles obtained with negative increments are different for

Table 6  
Statistical characteristics of the modeled skeletal mobility in i-PVA

Property\barrier	$\text{min}_1\text{--max}_1$	$\text{min}_2\text{--max}_2$	$\text{min}_3\text{--max}_3$	Total <sup>a</sup>
$E_a$ ( $\text{kJ mol}^{-1}$ )	$59(\pm 21)$	$58(\pm 19)$	$38(\pm 17)$	$52(\pm 23)$
% $t$ states for $\text{min}_i$	68	22	10	–

<sup>a</sup> Average value.

both the minima and maxima values. This situation is comparable to what was observed in the case of the phenyl rotation in polystyrene [18].

### 3.4.2. Calculated activation energies

The discontinuities observed in the total energy profile makes difficult the analysis used for the side chain motion. This is not surprising, as a two-sites jump model is not supposed to describe a cooperative motion. However, following Rapold and Suter [18], each transition barrier can be evaluated by taking the energy difference between the ground state, i.e. the minimum, and the maximum before the discontinuity. Each energy barrier ( $\min_i - \max_i$ , from  $i = 1, 2$  and  $3$ ; called barrier 1, 2 and 3, respectively) for each path, was evaluated on the fifty torsion angles. The corresponding activation energies distribution appears in Fig. 5. The average values are given in Table 6. The two first barriers have comparable average values of about  $60(\pm 20)$  kJ mol<sup>-1</sup>. This is much higher than the last average energy barrier which is about  $38(\pm 17)$  kJ mol<sup>-1</sup> but corresponds mainly in returning to the preferred *t* state. By taking into account all the 50 paths and all the energy barriers, an average value of 52 kJ mol<sup>-1</sup> is obtained. However, these energies are widely distributed, by about  $\pm 23$  kJ mol<sup>-1</sup>.

### 3.4.3. Comparison with experimental results

DMA of dried PVA shows a very broad peak corresponding to the secondary  $\beta$ -relaxation with an apparent activation energy of  $80(\pm 14)$  kJ mol<sup>-1</sup> and a short pre-exponential time ( $10^{-18}$  s), which indicates a certain motional cooperativity [21]. The calculated mean activation energy is slightly underestimated as compared to the experimental results, even if the width of the relaxation is well described. However, the calculated values are in the range of typical  $\beta$ -relaxation process [48,49].

Two main reasons should explain this difference. (i) When a relaxation is cooperative, and this is the case for the  $\beta$ -relaxation, it is difficult to assign the apparent activation energy to a single energy barrier. Indeed, the whole system

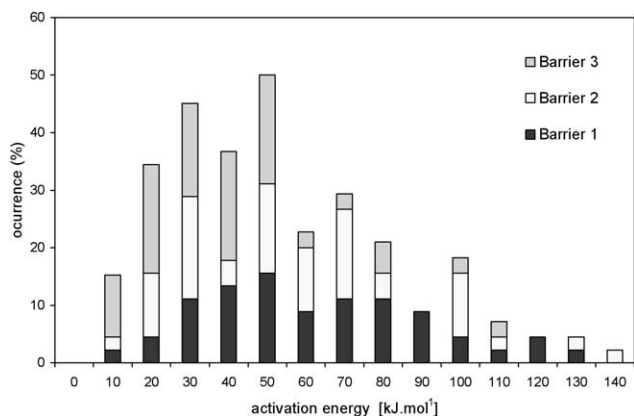


Fig. 5. Distribution of the energy barriers between two minima of the energy profile for the main-chain motions in i-PVA.

undergoes large conformational changes, and hence crosses several energy barriers. The entropy plays a non-negligible role. In that sense, the energy barrier calculated by molecular simulation would be the activation enthalpy as defined by Starkweather [50]. The way to account for the entropic contribution from the modeling data is not yet clear. However, following Starkweather calculations, the activation enthalpy is found around 60 kJ mol<sup>-1</sup>, in good agreement with the present calculated data. (ii) It should also be noticed that the averaging of the activation energies has been done by considering the equivalent contribution of each motion. However, it is generally admitted that the strength of a relaxation depends on the amplitude of the motion. Then, the impact of motions involving many bonds should be different in terms of contribution to the relaxation. For those reasons, a direct comparison between calculated and experimental results remains qualitative.

### 3.4.4. Cooperativity

The analysis of the skeletal torsion angles distribution for  $\phi_j$  (for  $j \neq i$ ) when a specific torsion angle  $\phi_i$  presents a conformational transition (i.e.  $\Delta\phi = 120 \pm 30^\circ$ ) reveals that at least one neighboring main-chain torsions angle is affected by this transition. Different variations of the whole skeletal torsion angles, when a specific conformational transition for  $\phi_i$  occurs, are shown in Fig. 6. These curves represent typical examples picked out of the fifty profiles. The forced motion of a torsion angle always implies a simultaneous conformational change of neighboring torsion angles. Various situations are encountered throughout the different profiles. In the first case (Fig. 6(a)), the transition between two states of the forced torsion angle ( $\phi_{105}$ ) implies a conformational change of the next neighbor torsion angle ( $\phi_{106}$ ) with an adaptation of three other torsion angles in the range of  $40^\circ$ . For the forced torsion angle ( $\phi_{90}$ ) (Fig. 6(b)), whose energy profile is shown in Fig. 4, a change of the second next neighbor torsion angle ( $\phi_{92}$ ) is observed. In addition, it necessitates a small rearrangement of ca.  $20^\circ$  of neighboring torsions (96, 101) and of distant (124, 195, 196) but spatially close torsions (Table 5). Three or four torsion angles can also be involved, as seen in Fig. 6(c) and (d), respectively. All types of motions are present: around 50% of the motions imply the change of two torsion angles, whereas motions involving three (35%) or more (15%) torsion angles are less represented.

Similarly, Fig. 7(a) and (b) show the variation of the side chain torsion angles ( $\omega_i$ , for  $i = 2, 4, \dots, 200$ ) along the chain, for the molecular motions shown in Fig. 6(b) and (c), respectively.  $\omega_{90}$  is the torsion angle defining the position of the side group attached to one of the central atom defining the  $\phi_{90}$  torsion. In both processes,  $\omega_{90}$  but also  $\omega_{68}$ , and  $\omega_{92}$  torsion angles present a conformational interconversion, i.e. a variation of  $120(\pm 30^\circ)$ . Additionally, six other torsion angles present an important variation (between 40 and  $80^\circ$ ). All these side groups are spatially close to the atoms

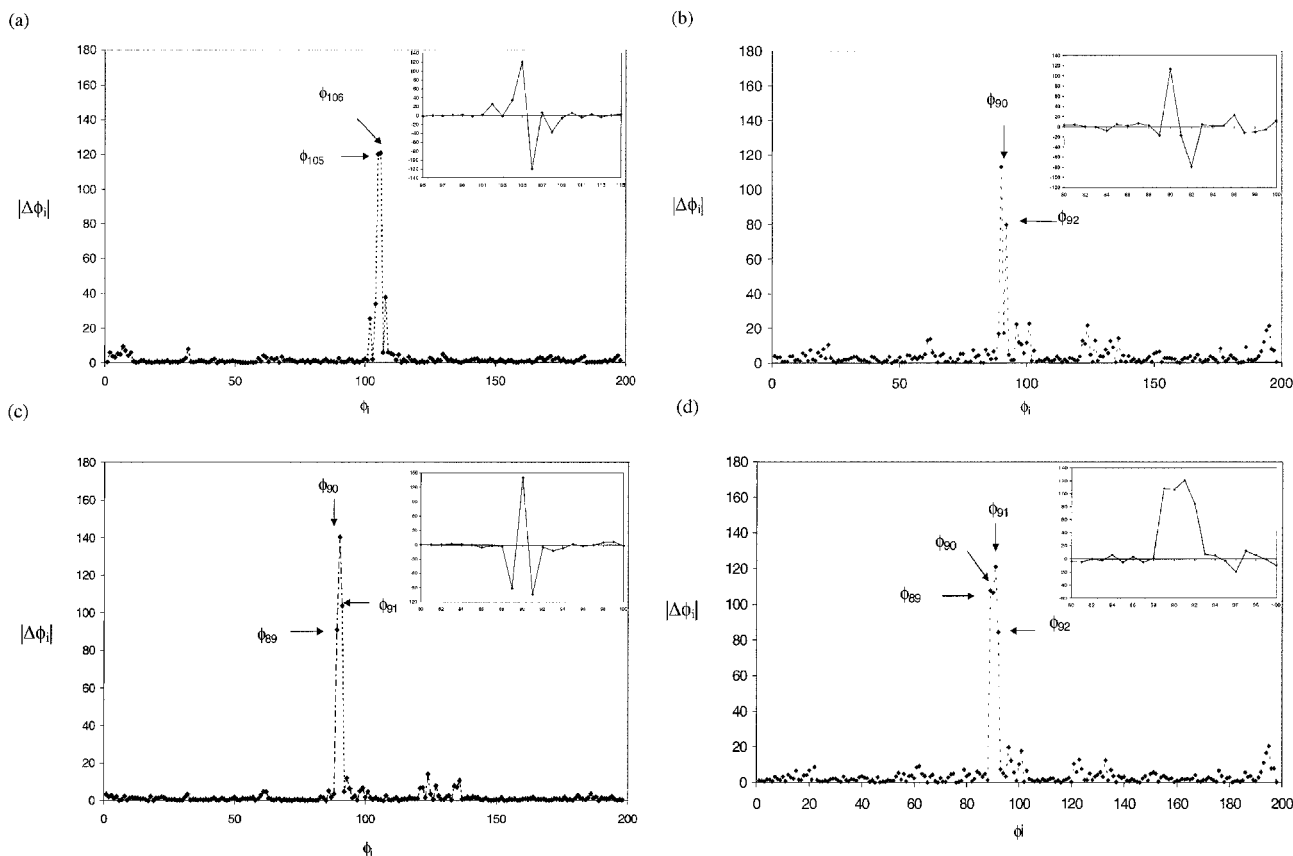


Fig. 6. Skeletal torsion angles changes  $|\Delta\phi_i|$  along the chain, when  $\phi_{105}$  undergo a conformational change from  $t$  to  $g^-$  state (a) and  $\phi_{90}$  from  $t$  to  $g^-$  state. (b) Skeletal torsion angles changes  $|\Delta\phi_i|$  along the chain, when  $\phi_{90}$  undergo a conformational change from  $g^-$  to  $g^+$  state (c) and from  $g^+$  to  $t$  state (d).

defining the  $\phi_{90}$  torsion and define a small volume affected by the motion.

This strongly suggests the cooperativity of the molecular motions. A possible explanation is that a new local equilibrium of amorphous state is reached during the conformational change. New orientations adopted by both skeletal and side group torsion angles define a new microstate with an energy value slightly different as compared to the previous one. This also explains the irreversibility of the quasi-static process. This interconversion between two microstates occur during the sharp discontinuities between  $\max_i$  and  $\min_{i+1}$ .

### 3.4.5. Geometry of the motions

Three distinct types of segmental motions have been proposed by Helfand [51], in which a limited number (one to five) of neighboring torsion angles are implied. The classification relies on the consequences experienced by the remaining part of the chain during the conformational change. Then, motions of type 1, including the ‘three bonds’ and ‘crankshaft’ motions do not imply a translational motion of the remaining part of the chain. Type 2 motions involve a small translation of one part of the chain, whereas those of type 3 necessitate a rotation. Motions of type 1 are supposed to be the easiest in terms of energy cost. Indeed,

the translation or the rotation of the chain implies a viscous friction, which is considered impossible for type 3 motions.

Surprisingly, each of the three types of motions is present in the calculated results. They are all represented by the skeletal torsion angles changes shown in Fig. 6. The motion implying the conformational change of two torsion angles (Fig. 6(a)) corresponds to a conversion from  $tg$  to  $gt$  pairs of conformations (constrained torsion in bold). They are classified in the type 3 motions, which should involve a rotation of the remaining part of the chain. To avoid this movement that is impossible in the glassy polymer, the constraint is released by contra-rotation of three of the neighbors. Type 2 motions are also present. Fig. 6(b) describes a transition from a  $tt$  to a  $g^-tg^+$  sequence known as a ‘gauche pair creation’. In Fig. 6(c) a conversion from a  $tg^-g^-$  to a  $g^+g^+t$  sequence (not described by Helfand) is shown for which the contra-rotation is clearly visible in the insert. The adaptation of the neighboring torsion angles is less pronounced than in the previous case (in the range of  $20^\circ$ ). Both types 2 and 3 represent around 80% of the studied cases. Finally, motions involving more than three torsions angles are also present but with a lower statistical weight. The example shown in Fig. 6(d) implies the conformational changes of four torsion angles and corresponds to a transition from a  $g^-g^-tg^+$  to a  $g^+g^+g^+t$  sequence. This unexpected presence of both type 2 and 3 motions

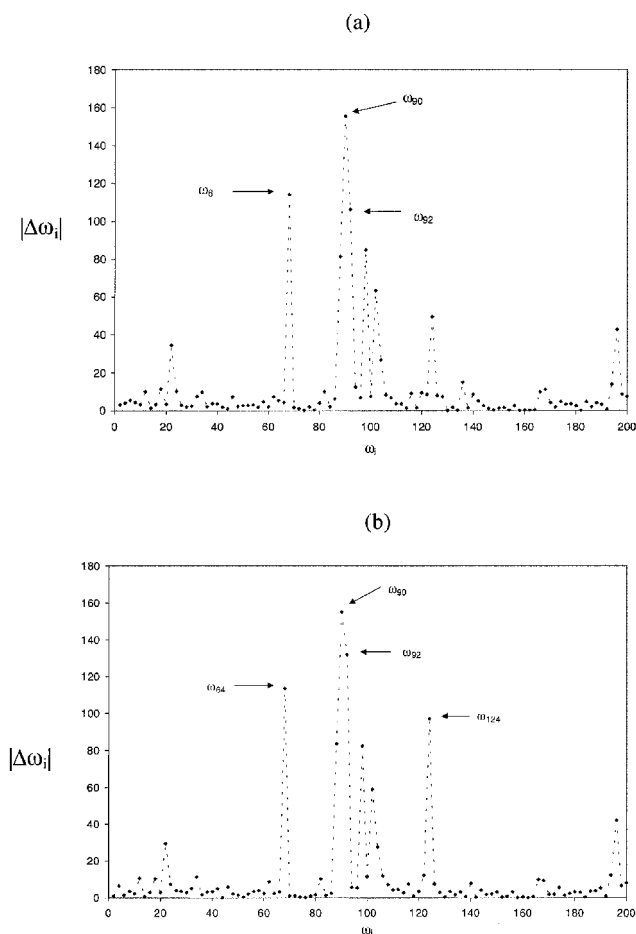


Fig. 7. Side chain torsion angles changes  $|\Delta\omega_i|$  along the chain, when  $\phi_{90}$  undergo a conformational change from  $t$  to  $g^-$  state (a) and from  $g^+$  to  $t$  state (b).

corresponds to what was observed by Brownian dynamics [52] and the cooperative kinematics theory [4] with about the same occurrence.

The presence of localized motions together with the partial rearrangement of the local neighborhood has two consequences. Firstly, as discussed below, it is a signature of the cooperative character of the motions implying conformational changes of the skeletal torsion angles. Secondly, as these motions have been described for the local mobility far above  $T_g$ , it supports the idea of the precursor character of the  $\beta$ -relaxation towards the glass transition [53]. These motions related to the  $\beta$ -relaxation are obviously more localized than those implied in the glass transition, but they apparently share some geometrical characteristics. The rearrangement of distant in the chemical structure but spatially close torsion angles of both the main-chain and the side groups implies also that a small volume is involved in the motion. This is close to the concept developed by Perez [53] of the ‘quasi-point defects’ relevant to describe molecular processes of mechanical relaxations. Indeed, the calculated results show that the rotation of a skeletal bond is impossible without shearing a

volume around the site where a conformational change occurs.

#### 4. Conclusions

The quasi-static method has permitted to precise some features concerning the localized molecular motion of vinyl polymers bearing polar groups. The energy profiles of the forced rotation of lateral groups agree with the idea of a two-site jump model, in which two equivalent positions are separated by an energy barrier. In the case of the hydroxymethyl group, the calculated data are in very good agreement with the activation energy of the macroscopic  $\gamma$ -relaxation process and thus confirm the attribution of this motion. This computational approach reinforces the hypothesis of a different motional behavior between hydroxyl and hydroxymethyl groups suggested by mechanical and dielectric spectroscopies. This supports as a general trend the conclusions originating from the comparison of different polymers bearing either hydroxyl (PVA, dextran) and hydroxymethyl (PAA, cellulose) side groups. The localized character of this type of motion is also clearly evidenced. Additional information that cannot be inferred from the experimental data is the number of relaxing sites. This should be useful to understand the origin of the experimental relaxation strength and its sensitivity to external parameters, like the water uptake.

Conversely, the forced motions of a skeletal bond appear more complex. The energy profiles obtained by a quasi-static method are discontinuous. The calculated activation energies of these motions are, however, compatible with the experimental values. The conformational transition of one bond involves both neighboring and remote but spatially close repeat units. The rotation of a skeletal bond is cooperative, localized but should correspond to local motion later involved in the glass transition. This type of behavior was already observed with other computational approach and correspond to a geometrical representation of the cooperativity concept.

This method has also some limitations as it does not allow the kinetic characterization of a given molecular motion. Additionally, complex motion involving many bonds cannot be described by this approach. In that sense, it could not be used to characterize all the molecular motion involved in a complex relaxation. It nevertheless described accurately localized motion. We then believe that a careful use of this method should bring energetic and geometrical information on the origin and modification of the molecular motions in the glassy state. As aforementioned, it could bring useful information on the role of water on the relaxation process. This latter phenomenon is of particular importance for polymers bearing polar groups (polysaccharides, polyamides, etc). Work is in progress to characterize this type of polymers with increasing water content.

## Acknowledgments

A. De La Rosa gratefully acknowledges CONACyT (Consejo Nacional de Ciencia y Tecnología) for the economic support during this work.

## References

- [1] Ediger MD, Adolf DB. *Adv Polym Sci* 1994;116:73–107.
- [2] Roe RJ. *Adv Polym Sci* 1994;116:111–43.
- [3] Bahar I, Erman B, Monnerie L. *Macromolecules* 1992;25:6309–14.
- [4] Bahar I, Erman B, Monnerie L. *Macromolecules* 1992;25:6315–21.
- [5] Bahar I, Erman B, Monnerie L. *Adv Polym Sci* 1994;116:145–203.
- [6] Hutnik M, Argon AS, Suter UW. *Macromolecules* 1991;24:5970–9.
- [7] Hutnik M, Argon AS, Suter UW. *Macromolecules* 1993;26:1097–108.
- [8] Fan CF, Tahir C, Chen ZM, Smith KA. *Macromolecules* 1994;27:2383–91.
- [9] Fan CF. *Macromolecules* 1995;28:5215–24.
- [10] Rapold RF, Suter UW, Theodorou DN. *Macromol Theor Simul* 1994;3:19–43.
- [11] Ogura I, Yamamoto T. *Polymer* 1995;36:1375–81.
- [12] Seung SJ, Won HJ. *Polymer* 1999;40:919–25.
- [13] Han J, Boyd RH. *Macromolecules* 1994;27:5365–70.
- [14] Knopp B, Suter UW, Gusev AA. *Macromolecules* 1997;30:6107–13.
- [15] Knopp B, Suter UW. *Macromolecules* 1997;30:6114–9.
- [16] Charati SG, Stern SA. *Macromolecules* 1998;31:5529–35.
- [17] Cuthbert TR, Wagner NJ, Paulaitis ME, Murgia G, D'Aguanno B. *Macromolecules* 1999;32:5017–28.
- [18] Rapold RF, Suter UW. *Macromol Theor Simul* 1994;3:1–17.
- [19] Montes H, Mazeau K, Cavaille JY. *Macromolecules* 1997;30:6977–84.
- [20] Montes H, Cavaille JY. *Polymer* 1999;40:2649–57.
- [21] De La Rosa A, Heux L, Cavaille JY. *Polymer* 2000;41:7547–57.
- [22] De La Rosa A, Heux L, Cavaille JY. *Polymer* 2001;42:5371–9.
- [23] Maple JR, Dinur U, Hagler AT. *Proc Natl Acad Sci USA* 1988;85:5350–4.
- [24] Maple JR, Hwang MJ, Stockfisch TP, Dinur U, Waldman M, Ewig CS, Hagler AT. *J Comput Chem* 1994;15:162–82.
- [25] Sun H, Mumby SJ, Maple JR, Hagler AT. *J Am Chem Soc* 1994;116:2978–87.
- [26] Sun H. *Macromolecules* 1995;28:701–12.
- [27] Gestoso P, Brisson J. *Comput Theor Polym Sci* 2001;11:263–71.
- [28] Trommsdorff U, Tomka I. *Macromolecules* 1995;28:6128–37.
- [29] Trommsdorff U, Tomka I. *Macromolecules* 1995;28:6138–50.
- [30] Nick B, Suter UW. *Comput Theor Polym Sci* 2001;11:49–55.
- [31] Wolf RM, Suter UW. *Macromolecules* 1984;17:669–77.
- [32] Modi TW. Polyvinylalcohol. In: Davidson RL, editor. *Handbook of water-soluble gums and resins*. New York: McGraw-Hill; 1980. p. 20–4.
- [33] Verlet L. *Phys Rev* 1967;159:98–103.
- [34] Parrinello M, Rahman A. *J Appl Phys* 1981;52:7182–90.
- [35] Nosé S. *Mol Phys* 1984;52:255–68.
- [36] Accelrys inc, San Diego, CA.
- [37] Robyr P, Tomaselli M, Grob-Pisano C, Meier BH, Ernst RR, Suter UW. *Macromolecules* 1995;28:5320–4.
- [38] Kotelyanskii M, Wagner NJ, Paulaitis ME. *Macromolecules* 1996;29:8497–506.
- [39] Paul W, Smith GD, Yoon DY. *Macromolecules* 1997;30:7772–80.
- [40] Robyr P, Muller M, Suter UW. *Macromolecules* 1999;32:8681–4.
- [41] Flory PJ. *Principles of polymer chemistry*. Ithaca, NY: Cornell University Press; 1953.
- [42] Flory PJ. *Statistical mechanics of chain molecules*. New York: Interscience; 1969.
- [43] Mattice WL, Suter UW. *Conformational theory of large molecules*. New York: Wiley; 1994.
- [44] Ludovice PJ, Suter UW. Detailed molecular structure of a polar vinyl polymer glass. In: Bicerano J, editor. *Computational modeling of polymers*. New York: Marcel Dekker; 1992. p. 401.
- [45] Theodorou DN, Suter UW. *Macromolecules* 1985;18:1467–78.
- [46] Shvarts AG. *Kolloid Zh* 1956;18:755–61.
- [47] Horii F, Hu S, Ito T, Odani H, Kitamaru R, Matsuzawa S, Yamaura K. *Polymer* 1992;33:2229–306.
- [48] Heijboer J. *Midland macromolecular monographs*. New York: Gordon & Breach; 1975.
- [49] Heijboer J, Baas JMA, Van de Graaf B, Hoefnagel MA. *Polymer* 1987;28:509–13.
- [50] Starkweather HW. *Macromolecules* 1981;14:1277–81.
- [51] Helfand E. *J Chem Phys* 1971;54:4651.
- [52] Helfand E, Wasserman ZR, Weber TA. *Macromolecules* 1980;13:526–33.
- [53] Perez J. *Physique et Mecanique des Polymeres Amorphes*. Paris: Ted Lavoisier; 1992. p. 384.